

# An experimental study of a two-dimensional plane turbulent wall jet

J. G. Eriksson, R. I. Karlsson, J. Persson

50

**Abstract** Laser-Doppler measurements were conducted in a plane turbulent wall jet at a Reynolds number based on inlet velocity,  $Re_0$ , of 9600. The initial development as well as the fully developed flow was studied. Special attention was given to the near-wall region, including the use of small measuring volumes and the application of specific near-wall data corrections, so that wall shear stresses were determined directly from the mean velocity gradient at the wall using only data below  $y^+ = 4$ . It was possible to resolve the inner peak in the streamwise turbulence intensity as well as the inner (negative) peak in the shear stress. Limiting values of  $(u')^+$  and  $uv^+$  were determined. Turbulence data from the outer region of the flow were compared to earlier hot wire measurements and large differences in the normal turbulence intensity and the shear stress were found. These differences can be attributed to high turbulence intensity effects on the hot-wires.

## 1

### Introduction

Following Launder and Rodi (1981), hereafter referred to as LR81, a wall jet may be defined as “a shear flow directed along a wall where, by virtue of the initially supplied momentum, at any station, the streamwise velocity over some region within the shear flow exceeds that in the external stream”. Wall jets are of great engineering importance with many applications. Some examples are defrosters in automobiles where wall jets are used for mass transfer modifications, and aero engines and stationary gas turbines, where wall jets are used for cooling of combustion chamber walls and the leading stages of the turbine itself.

*Received: 17 October 1996 / Accepted: 8 December 1997*

J. G. Eriksson, R. I. Karlsson<sup>1</sup>, J. Persson  
Vattenfall Utveckling AB, S-814 26 Älvkarleby, Sweden

<sup>1</sup>Department of Mechanics/Hydronechanics, the Royal Institute of Technology, S-100 44 Stockholm, Sweden

*Correspondence to:* R. I. Karlsson

The authors are grateful to Professors William K. George of the State University of New York at Buffalo and Arne V. Johansson of the Royal Institute of Technology at Stockholm for several discussions and helpful comments on draft versions of this paper. Professor Lennart Löfdahl and Dr. Hans Abrahamsson at Chalmers University of Technology, Gothenburg, freely shared their experimental data with us.

The turbulent wall jet is also a basic flow of fundamental interest for turbulence researchers because of its two-scale character. The inner layer of the plane wall jet is similar to that of the turbulent boundary layer, while the outer layer resembles that of a free (plane) jet. The interaction of large turbulence scales in the outer layer with smaller scales in the inner layer creates a complicated flow field and determines the development of the wall jet. The flow situation is sketched in Fig. 1.

Due to the many applications of wall jets, the literature is immense. Launder and Rodi (1981, 1983) reviewed the experimental literature up to 1980. Reviews of the more recent literature are found in eg. Abrahamsson et al. (1994) and George et al. (1997).

Recent major experimental studies of turbulent wall jets are the work by Wygnanski et al. (1992) and Abrahamsson et al. (1994) who used HWA to study the wall jet in stagnant surroundings, and the work by Schneider (Schneider 1987; Schneider and Goldstein 1994), who used residence-time-weighted LDV. A recent theoretical work is that by George et al. (1997), hereafter referred to as GAELK. Earlier results of this work has been reported in George et al. (1996) and in Abrahamsson (1997).

The main purpose of the present paper is to provide a comprehensive data set on mean velocities and turbulence structure for the wall jet, and to present new near-wall data obtained with high spatial resolution using LDV. Where relevant, the results will be compared to the similarity theory for the plane wall jet proposed in GAELK. Following this introduction, the test facility is described together with the instrumentation used and the experimental procedure followed. Results are given both for the initial development of the flow and for the developed region, with emphasis on the latter. Turbulence data are treated in some detail.

The experiments were performed in 1991, and a small part of the results, together with some aspects of the experimental methodology, were presented by Karlsson et al. (1993a). The experimental data were compiled and reported by Karlsson et al. (1993b) and are available in the ERCOFTAC Data Base. The data have also been used as a test case in the ERCOFTAC/IAHR Workshops on Refined Turbulence Modelling in Paris, 1996 and in Delft, 1997.

## 2

### Experimental apparatus and procedure

The basic flow field that we have tried to obtain is the two-dimensional wall jet on a plane surface, and more

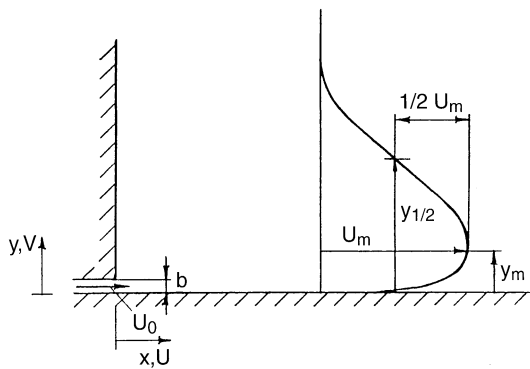


Fig. 1. Configuration and nomenclature for the plane wall jet

specifically “the plane wall jet in still air” according to the terminology used by LR81. There are, however, variations also on this subsection of the wall jet. These variations concern the design of the wall above the inlet. This wall is usually either a thin lip, used e.g. in the experiment by Wagnanski et al. (1992), or an “infinite” vertical wall as in the present experiment. The latter design is simpler to treat computationally, since it, together with a “no inflow” – upper boundary, results in a single, well-defined inflow boundary with known boundary conditions. It was therefore chosen here, in spite of the inevitable return flow that this configuration generates, a return flow which far downstream of the nozzle changes the character of the jet.

An important criterion in the experimental design was that the spatial resolution should be sufficiently high to allow the wall shear stress to be determined directly from mean velocity measurements. This imposes an upper limit on the ratio of measuring control volume diameter to viscous length scale, but a high enough inlet  $Re$ -number must also be retained to allow comparisons with earlier studies. Once water was chosen as the working fluid, due to the absence of seeding problems in low-speed water flows, these considerations led to the present combination of slot width and inlet velocity.

## 2.1 Wall jet test facility

The test facility is shown in Fig. 2. It consists of a large tank into which a jet discharges. The tank is 7 m long and its width is

1.45 m. One of the side walls is made of glass, as well as the bottom. (Using a glass bottom improves the conditions for near-wall measurements, since its smoothness minimizes the diffuse surface reflections. (Johnson and Brown 1990).)

The slot height was measured with water in the tank, by a diver. The results showed the slot height to be  $9.6 \pm 0.1$  mm over most of the slot width. Given the uncertainties involved, this is consistent with an indirect determination of the slot height using the volumetric flow rate. Consequently,  $b = 9.6$  mm will be used in the following analysis, giving a jet width-to-height ratio of 151. This was considered large enough to obtain good two-dimensionality. A large contraction (Morel 1975) with a turbulence-reducing screen inserted is used to produce a fairly flat mean velocity profile at the inlet. A weir upstream of the contraction keeps the upstream water level constant, and the flow velocity through the slot is set by an adjustable weir at the downstream end at the tank. This reference velocity is determined as

$$U_0 = \sqrt{2g \Delta h} \quad (2.1)$$

where  $\Delta h$  is the difference in height between the upstream and downstream free surfaces.

The inlet velocity,  $U_0$ , was set as close as possible to 1 m/s, corresponding to a water depth downstream of the inlet of about 1.4 m. For this water depth, the influence of the recirculating flow on the growth rate of the jet was negligible for the first 150 slot heights.

Using water of approximately room temperature, one obtains a nominal inlet  $Re$ -number

$$Re_0 = \frac{U_0 b}{\nu} \approx 9.6 \times 10^3 \quad (2.2)$$

which is sufficiently high to be comparable to previous experimental studies, e.g. Bradshaw & Gee (1960) and Tailland and Mathieu (1967).

## 2.2 Instrumentation

The LDV hardware consisted of a modified TSI two-colour system (TSI 9100-7) together with TSI 1980 counter signal processors and frequency shift modules. The system was modified as to increase the beam expansion ratio to 8.5 by including an extra beam expansion module. An upper-central beam arrangement was used to measure the normal velocity

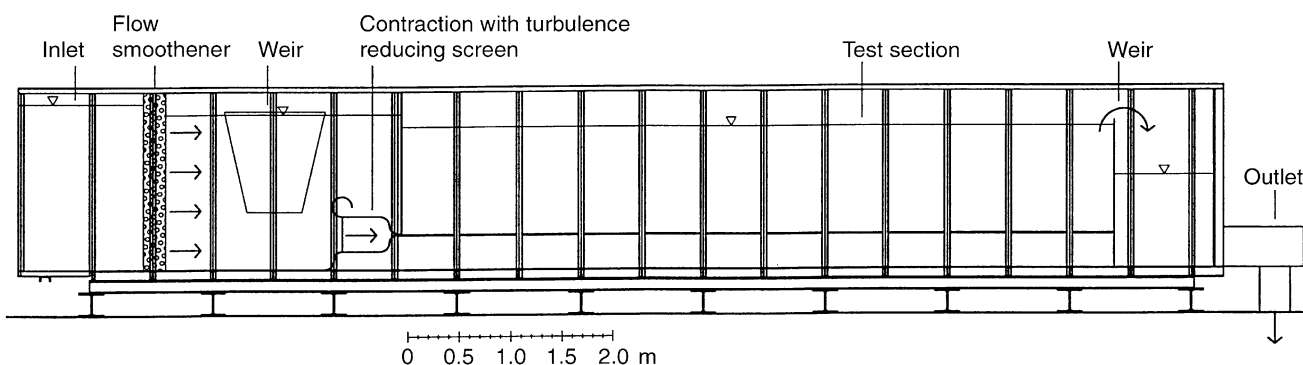


Fig. 2. Wall jet test facility

component ( $V$ ), see Karlsson and Johansson (1988). A front lens with a focal distance of 750 mm was used, in order to reach the centreline of the tank. The measuring volume sizes were  $(0.73 \times 0.05)$  mm (streamwise velocity component – 488 nm) and  $(1.60 \times 0.05)$  mm (normal velocity component – 514.5 nm), respectively. Standard TSI software running on a DEC PDP 11 was used for data collection and reduction. Silicon carbide particles with a mean diameter of 1.5  $\mu\text{m}$  was used to uniformly seed the flow.

During all measurements, the counters were operated as free-running processors and multiple measurements per burst (MMPB) were permitted. No post-facto velocity bias eliminating algorithms have been applied. The available implementation of the residence time weighting was not used since an analysis of the measurement situation showed that erroneous residence time computations could be expected due to hardware limitations. However, Meyers and Clemmons (1979) have shown that the use of the MMPB-mode significantly reduces the velocity bias. George (personal communication) has pointed out the equivalence of this technique to residence time weighting, since the velocity of each particle is effectively “weighted” by the length of time it is present in volume.

With the exception of the positions closest to the wall, where only the streamwise velocity component was measured, all measurements were made in coincidence mode; i.e. requiring the bursts in channel 1 and channel 2 to arrive within a certain, pre-determined time interval. Shift frequencies were chosen such that all likely flow angles were measured with equal probability (Whiffen 1975; Buchhave 1975, 1979), while still staying away from the filter limits.

## 2.3

### Experimental procedure and flow qualification

#### 2.3.1

##### Outline of measurements

Extensive Pitot-tube measurements, spanwise profiles at several heights and numerous vertical profiles at different spanwise positions, were made at the slot ( $x=0$ ) to check for symmetry and spanwise variations. Part of the inlet velocity profile was also measured using LDV, to better resolve the boundary layer and to get turbulence data. LDV measurements, streamwise and spanwise profiles, were also taken immediately downstream of the slot.

Extensive spanwise measurements were made at several streamwise positions in order to check the two-dimensionality of the flow. Based on these spanwise measurements, it was decided to make the main measurements series approximately halfway between the centre-line and the glass wall. The flow conditions in that spanwise position were identical to those at the centre-line within the measurement accuracy.

The main measurement series were taken at the following streamwise positions:  $x = 50, 100, 200, 400, 700, 1000, 1500, 2000$  mm. For the sake of simplicity, we will refer to these positions as  $x/b = 5, 10, 20, 40, 70, 100, 200$ , although the actual dimensionless distance was about 4% larger. In figures showing the streamwise development of a quantity, the correct  $x/b$  will be used. Measurements stopped at  $x/b = 200$  because the flow was losing its wall-jet character. This issue will be discussed later on.

#### 2.3.2

##### Main measurement series

The vertical profiles of the main measurement series were taken in order from  $x/b = 5$  and downstream.  $\Delta h$  and the water temperature,  $T_0$ , was checked regularly, in order to detect any drift in inlet velocity or inlet  $Re$ -number. There was essentially no change in  $U_0$  or  $Re_0$  during the individual profiles. There were, however, small variations between the different profiles due to a 3% variation in the boundary conditions, i.e.  $Re_0$ . Where relevant, all velocities have been normalized to the same inlet velocity by multiplying with  $[U_0(x=0)/U_0(x=X)]$ .

The LDV system was slightly tilted relative to the  $z$ -axis. Typical tilt angle was  $1.5^\circ$ , referring to the central beam inside the tank. With the upper-central beam arrangement for the measurement of the normal velocity component, this configuration permitted velocity measurements very close to the surface. Typical minimum wall distance for simultaneous two-component measurements was 0.10–0.15 mm. When measuring only the streamwise velocity, it was usually possible to start at a wall distance of 0.05 mm. Since this made it possible to extend the measurements into the viscous sublayer, the wall shear stress could be determined directly from the mean velocity gradient.

The wall distance was determined in the following way: The position of the wall,  $y=0$ , was estimated by observing the output signal from the counter, i.e. after amplifying and filtering, on an oscilloscope. The “wall signal” is very characteristic. The distance from this preliminary wall position was then measured by a dial gauge. Finally, the wall distance was adjusted after the measurements by shifting the velocity curve up or down to make it pass through origin. This was relatively simple due to the linear relation. The necessary adjustments typically were of the order of 0.02 mm. An example of the resulting mean velocity distribution close to the wall was shown in Karlsson et al. (1993a). We estimate the remaining uncertainty in the wall distance to be  $\pm 0.01$  mm.

When simultaneous two-component measurements were made, 20480 samples were collected. This made for typical measuring times of 20 min per data point. During the one-component measurements very near the wall, either 5120 or 10240 samples were taken.

#### 2.3.3

##### Inlet conditions

The inlet conditions were determined using Pitot tube- and LDV-measurements. Mean velocity profiles from Pitot tube measurements, taken at several spanwise positions at and around the spanwise position finally chosen for the main measurements, showed no visible differences in the maximum velocity. There were, however, small differences in the length of the flat parts of the profiles. These are consistent with the earlier statement of a  $\pm 0.1$  mm variation in slot height. The variation in the spanwise velocity distribution at  $y = 4.5$  mm was less than  $\pm 0.25\%$ .

LDV measurements of the lower part of the inlet velocity profile were made in order to resolve the boundary layer and to obtain information on the turbulence levels. Mean velocities and turbulence intensities are shown in Fig. 3. The boundary

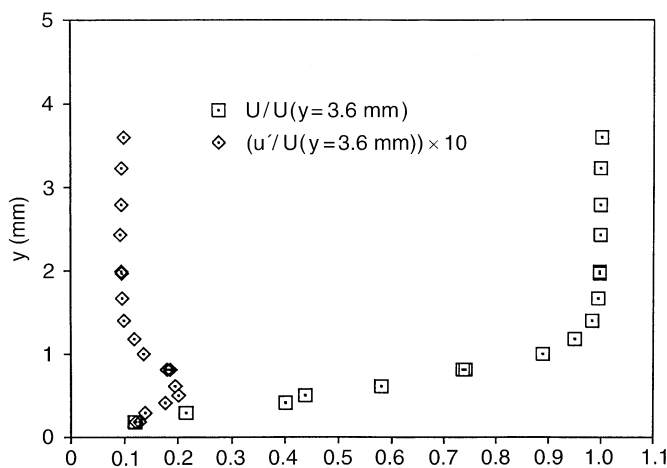


Fig. 3. Mean velocity and turbulence intensity profiles at inlet. LDV measurements

layer thickness, defined as  $U=0.99U_{\max}$ , is  $\sim 1.4$  mm. The turbulence intensity in the flat part of the profile is less than 1%. No corrections for gradient broadening has been applied to the turbulence measurements, meaning that the peak in turbulence intensity in the boundary layer is exaggerated.

We thus have a fairly flat inlet velocity profile with a mean velocity which is uniform in the spanwise direction within  $\pm 0.25\%$ . The flow is laminar and the laminar boundary layers along the walls have a thickness ( $\delta_{99}$ )  $\approx 1.4$  mm.

### 2.3.4

#### Two-dimensionality

Persistent spanwise variations of the thickness of the wall jet were noted. These variations are probably associated with the small variation ( $\pm 1\%$ ) in slot height. All subsequent measurements were however made at a spanwise position where “average properties” of the wall jet were prevailing.

## 3

### Experimental results

#### 3.1

##### Initial development

At  $x=0$ , the wall jet is laminar with thin laminar boundary layers (Fig. 3). The evolution of the flow down to  $x/b=40$  is shown in Fig. 4a–e.

At  $x/b=5$ , the mean velocity profile is laminar, but  $\overline{uv}$  is building up in the outer part of the jet, as is  $u'$  and  $v'$ . There is an inner layer peak as well in  $u'$ , but it is much smaller than the outer peak. (For the outer peak,  $u'/U_m \approx 0.22$ ).  $V/U_m > 0$ , indicating growth of the laminar boundary layer. Taken together, this suggests that transition starts in the outer part of the wall jet.

The data at  $x/b=10$  shows a transitional mean velocity profile. The shear stress has increased and  $V$  is negative in the vicinity of the wall, suggesting start of transition at the wall also. (An increased velocity gradient at the wall, a sure sign of transition, must be accompanied by an inflow of mass if continuity is to be fulfilled, given that the maximum velocity does not change appreciably). Also noted is an inner negative

peak in  $\overline{uv}$ , overshooting  $-\overline{uv}/(u^*)^2=1$ , and an outer positive peak about three times larger than the inner peak. The inner peak in  $u'$  is obvious.  $v'$  shows a plateau in the region  $50 < y^+ < 150$ , whereas  $u'$  has a minimum around  $y^+=150$ . Thus, two regions for production of turbulent kinetic energy are at work.

At  $x/b=20$ , we begin to reach a fully turbulent regime. The inner peak in  $u'$  at  $y^+ \approx 15$  is more accentuated, and the plateau in  $v'$  has disappeared. This means that the merging process of the inner and outer layer is well under way.

At  $x/b=40$ , finally, the transition to turbulent flow seems to be completed. The mean velocity profile is well developed, as well as the turbulence profiles. The turbulent shear stress,  $\overline{uv}/(u^*)^2$ , has a negative peak of about  $-1$  at  $y^+ \approx 30$  and a positive peak of about 4. Hence, the inner part has developed into a form closely resembling a zero-pressure-gradient turbulent boundary layer.

### 3.2

#### The developed region in outer scaling

##### 3.2.1

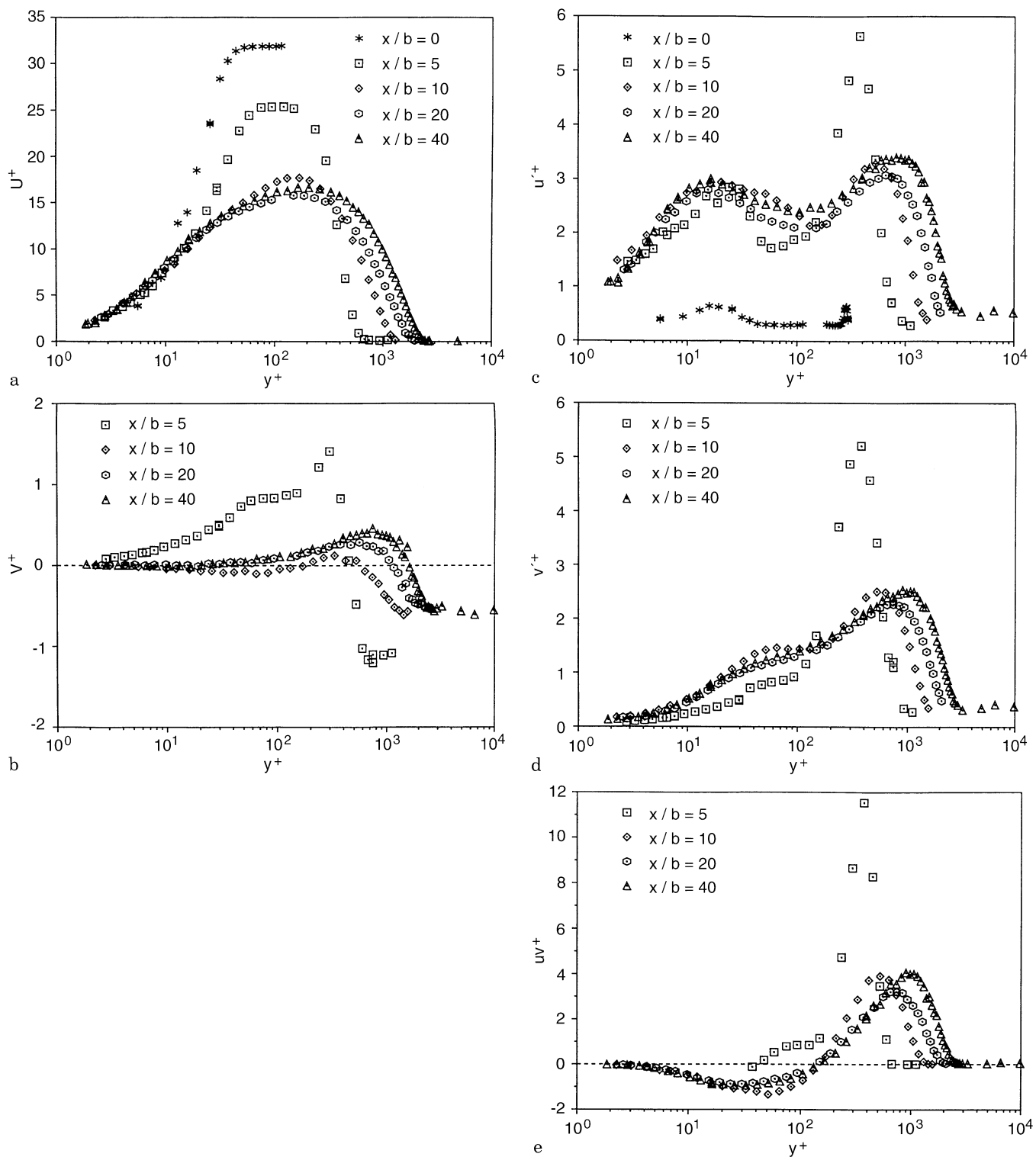
##### Mean velocity in outer variables

Figure 5 shows the mean velocity profiles from  $x/b=20$  to  $x/b=200$  in dimensionless form. The traditional outer scaling,  $U_m$  and  $y_{1/2}$ , is used. The collapse of data when using this scaling has been reported by many previous investigators, e.g. LR81. What should be noted here is the distinctly different appearance of the  $x/b=200$  – profile. At this position, the influence of the return flow clearly has changed the character of the wall jet. As a consequence, this profile will not be used when computing growth rate, skin friction, etc. On the other hand, there is an excellent collapse of data from  $x/b=20$  to  $x/b=150$  (with the possible exception of the outermost part of the profile at  $x/b=150$ ).

An often quoted parameter is  $y_m/y_{1/2}$ , the ratio of the distance of the velocity maximum from the wall to the jet half-width. The values quoted in LR81 ranges from 0.13 to 0.17. In the present investigation, this ratio is approximately 0.17, the same value as reported by Schneider and Goldstein (1994).

Figure 6 shows the dimensionless growth rate of the wall jet, in terms of jet half-width. Assuming a linear relation, a least-squares fit was applied to the data (starting with the position  $x/b=20$ ). The resulting rate of spread,  $dy_{1/2}/dx$ , is approximately 0.078, which does not fall within the range  $dy_{1/2}/dx=0.073 \pm 0.002$  given in LR81 for experiments satisfying momentum conservation. Since the present experiment does satisfy the momentum integral equation (as will be shown later), there is no reason to question the result because of this discrepancy. Furthermore, since the review papers by Launder and Rodi, data has been published that indicates a dependence of  $dy_{1/2}/dx$  on inlet  $Re$ -number, e.g. Abrahamsson et al. (1994). This is consistent with the theoretical argument by GAELK, who also argue that  $dy_{1/2}/dx$  is never independent of  $x$ .

If a power law relation is assumed instead of a linear relation, the  $x$ -exponent for the present data is found to be  $\sim 0.95$ , which is consistent with a non-linear growth. On the other hand, given the small difference between 0.95 and 1, and the sensitivity of the exponent to which data points are



**Fig. 4.** Mean velocities, turbulence intensities and shear stress in developing region,  $x/b = 0, 5, 10, 20$  and  $40$ . Inner scaling is used. **a**  $U^+$  vs.  $y^+$ , **b**  $V^+$  vs.  $y^+$ , **c**  $(u')^+$  vs.  $y^+$ , **d**  $(v')^+$  vs.  $y^+$ , **e**  $(\overline{uv})^+$  vs.  $y^+$

included in the curve fit, it is perhaps safest to say that the data are not completely conclusive concerning linear growth or not.

According to GAELK, a similarity solution to the momentum equation for the plane turbulent wall jet is possible only if

$$U_m = B(y_{1/2})^n \quad (3.1)$$

Figure 7 plots  $\log U_m$  versus  $\log y_{1/2}$ . It is seen that the data are in excellent agreement with the theoretical prediction over the range  $x/b = 40$  to  $x/b = 150$ ; i.e. over the part of the flow which, on one hand, is fully developed and, on the other hand, has not lost any noticeable amount of momentum to the return flow. For this data, the value of  $n$  is  $\approx -0.57$ . According to the theory, this should not be expected to be universal since

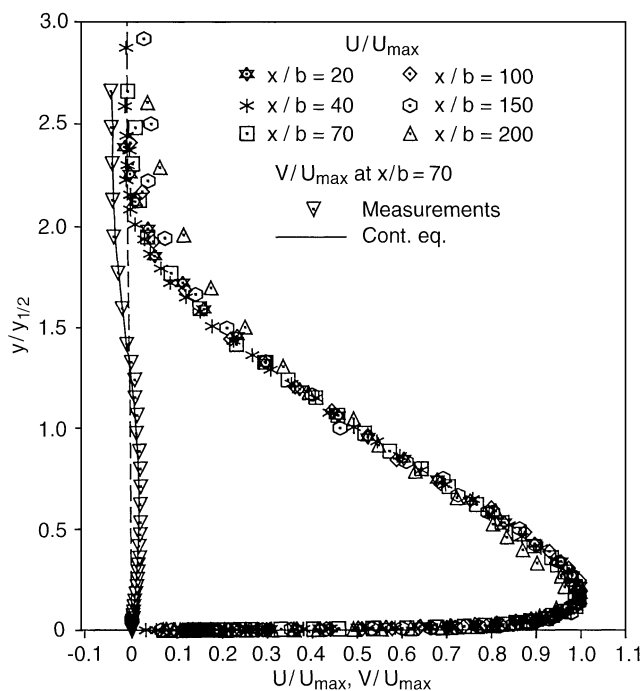


Fig. 5. Mean velocity profiles in outer scaling,  $U/U_m$ ,  $V/U_m = f(y/y_{1/2})$

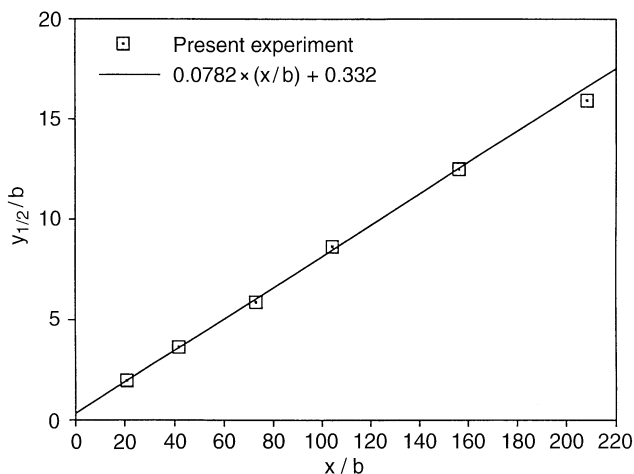


Fig. 6. Growth rate of wall jet. Linear relation assumed

it probably is dependent on source conditions. It should, however, always be less than  $-\frac{1}{2}$ .

### 3.2.2 Continuity

Also shown in Fig. 5 is  $V/U_m$  at  $x/b=70$ , as measured and computed from the continuity equation using similarity assumptions. This good agreement is typical of the positions  $x/b=20, 40$  and  $70$ . From  $x/b=100$  and downstream, larger differences between the peak values of the curves are seen. The curve forms, including the position for  $V=0$ , is still in very good agreement. The discrepancies starting at  $x/b=100$  could be due either to lower quality  $V$ -data or the beginning of loss of self-similarity.

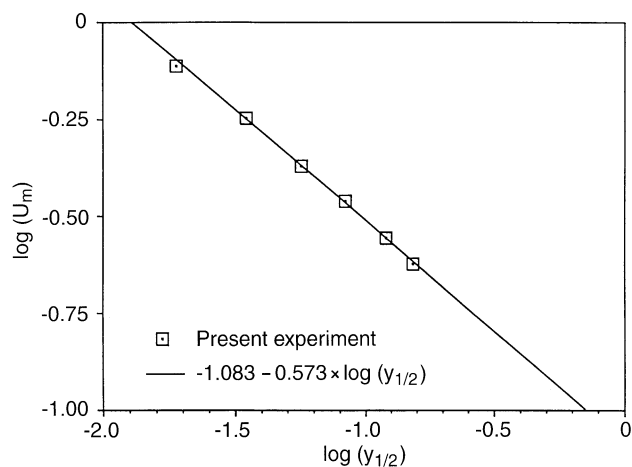


Fig. 7. Decay of streamwise mean velocity.  $\log U_m$  versus  $\log y_{1/2}$

### 3.2.3

#### Turbulence quantities in outer variables

The normal stresses as measured, normalized by  $U_m^2$ , showed a clear variation with streamwise position downstream of  $x/b=70$ , the turbulence levels increasing with distance from the inlet. A similar behaviour, but to a lesser degree, was seen for the Reynolds stress  $\overline{uv}$ . This is most probably due to the influence of the return flow. If we assume the flow field to be made up by two parts, a wall jet and a secondary flow uncorrelated with the jet, we can compute the turbulence due to the jet by subtracting the variance of the secondary flow from the measured variance. Assuming the “extra” turbulence at each streamwise position to be equal to the measured variance outside the jet at the same position, and using the level at  $x/b=40$  as reference, a reasonable collapse is achieved. (This procedure will lead to an overcorrection for small values of  $y$ . That should, however, not be a major inconvenience, since we presently are not concerned with that region.) The turbulence profiles so computed are shown in Figs. 8a–c. The near-wall peaks in  $\overline{u^2}$  and  $\overline{uv}$  are clearly seen.  $\overline{v^2}$ , on the contrary, increases monotonically to its peak level corresponding to the outer shear layer. This peak, as well as the outer peak in  $\overline{u^2}$ , is positioned at  $y/y_{1/2} \approx 0.7$ .

Also plotted in Fig. 8a–c are the HWA-data of Abrahamsson et al. together with an indication of the spread in earlier published HWA-results, taken from LR81. (Measurements deemed unreliable by them are not included. A consequence of this is the apparently small scatter in  $\overline{uv}$ , which simply reflects the fact that there were at that time very few shear stress measurements not obviously in error.) The data from Abrahamsson et al. has been chosen to illustrate “typical” HWA-results since it is a recent and very complete investigation, with inlet conditions very similar to the present investigation. The most striking features of this comparison, apart from the spread in  $\overline{v^2}$  on the HWA-data, are the large differences in  $\overline{v^2}$  and  $\overline{uv}$ , starting at about  $y/y_{1/2}=0.5$ , between the present measurements and those by Abrahamsson et al. Out peak values are 40% and 20% higher, respectively, and positioned further out. At  $y/y_{1/2}=1.0$ , the shear stress determined using LDV is 50% higher whereas the normal fluctuation is almost

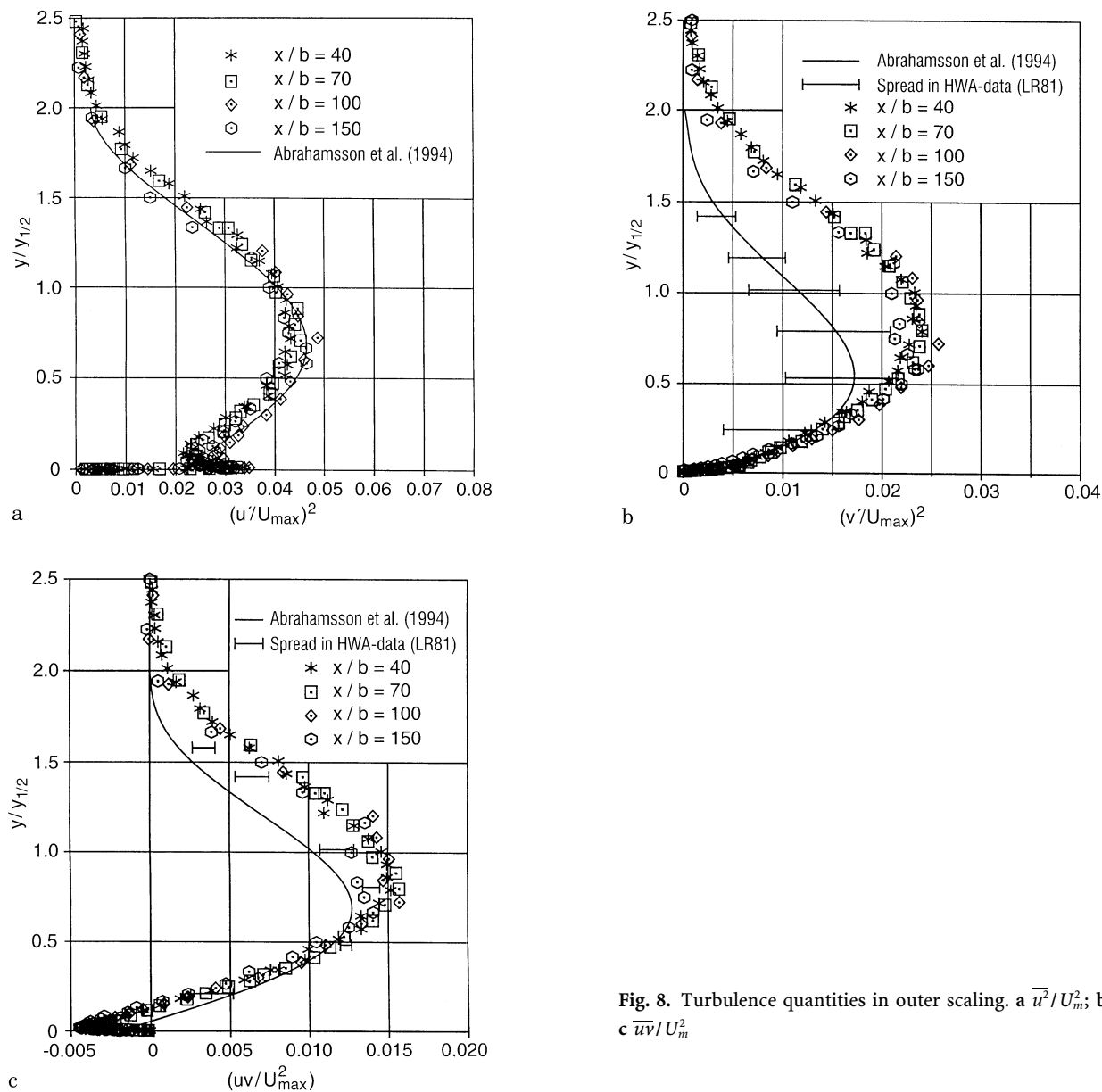


Fig. 8. Turbulence quantities in outer scaling. a  $\overline{u^2}/U_m^2$ ; b  $\overline{v^2}/U_m^2$ ; c  $\overline{uv}/U_m^2$

twice as high. Further out, the data of Abrahamsson et al. goes to zero much faster than the present data. Eriksson et al. (1997) show that these differences can be attributed to the high turbulence intensity effects on the hot-wires in the outer flow.

As a last item on the outer scaling, Fig. 9 shows the Reynolds stress scaled by  $u^{*2}$  and  $y_{1/2}$  which according to GAELK is the correct outer scaling for this quantity. It is impossible to draw any firm conclusions whether this scaling collapses the data better than the scaling used in Fig. 8c, in part because of the scatter in the data and in part because  $u^*/U_m$  is itself nearly constant. The HWA-data by Abrahamsson et al., which has much less scatter, does support the use of the friction velocity as the scaling parameter for the shear stress (George et al., 1996).

### 3.2.4 Skin friction

The wall shear stress,  $\tau_w$ , was determined from measurements of the velocity gradient at the wall,  $\tau_w = \mu(dU/dy)_{y=0}$ . Repeated

measurements of the very near-wall region were performed in order to confirm the procedure used. Figure 10 shows experimental data together with a linear velocity profile  $U^+ = y^+$ , and the theoretical velocity profile near the wall  $U^+ = y^+ + C_4 y^{+4}$ . The linear velocity profile alone appears to fit the data out to  $y^+ = 3-4$ , whereas the fourth order fit is good out to  $y^+ = 6-7$ . Our best estimate for the coefficient of the fourth order term is  $C_4 = -0.0003 (\pm 0.0001)$  meaning that at  $y^+ = 5$ ,  $U^+$  is down 4% compared to the linear estimate.

Local skin friction coefficients versus  $Re_m = U_m y_m / \nu$  are shown in Fig. 11.<sup>1</sup> The correlation proposed by Bradshaw and

<sup>1</sup>Correlating against  $Re_\delta = U_m y_{1/2} / \nu$  would be preferable, since  $y_{1/2}$  is easier to determine accurately.  $Re_m$  is used to facilitate comparison with previously published results. Note also that GAELK, from a theoretical point of view, proposes correlating  $C_f$  against  $y_{1/2}^+ = u^* y_{1/2} / \nu$ .

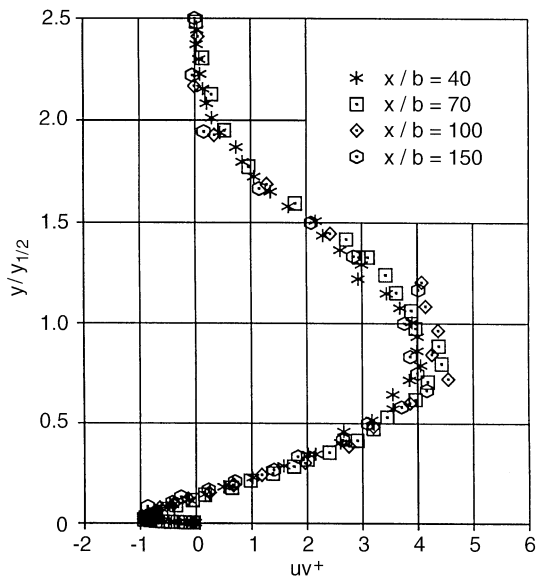


Fig. 9. Shear stress scaled according to GAELK,  $\overline{uv}/u^*$

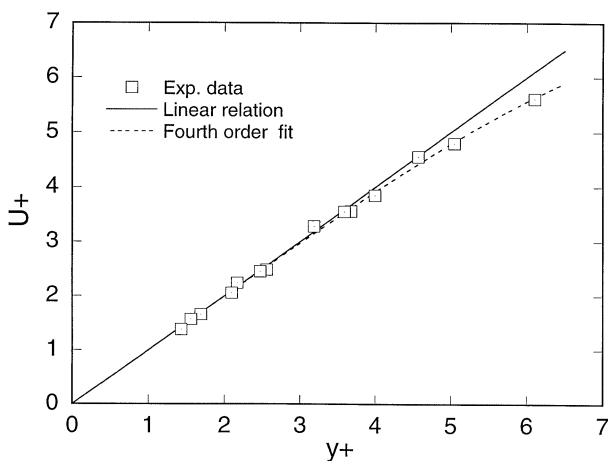


Fig. 10. Mean velocities in very near-wall region. Lines showing  $U^+ = y^+$  and  $U^+ = y^+ + C_4 y^{+4}$  included

Gee (1960), and recommended by LR81,  $C_f = 0.0315 Re_m^{-0.182}$ , is shown for comparison, as well as data from Abrahamsson et al. (1994), Wygnanski et al. (1992) and Tailland and Mathieu (1967). (Wygnanski et al. reported only their data points. We have tried to fit a line to their data, and it is this line that is shown in Fig. 11.)

The present data is in the range of the Bradshaw and Gee correlation in the limited range of  $Re$ -numbers studied, but shows a distinctly different  $Re$ -number dependence. A good empirical correlation of the present data is given by  $C_f = 0.0179 Re_m^{-0.113}$ .

In contrast to the present data, LR81 noted that the then existing determinations of  $C_f$  based on direct measurements of the mean velocity gradient at the wall produced values ranging from 20% to 35% below the consensus of the impact-tube data. The data from Wygnanski et al. (1992) and Tailland and Mathieu (1967) do show considerably lower skin friction coefficients than the present investigation. In both those

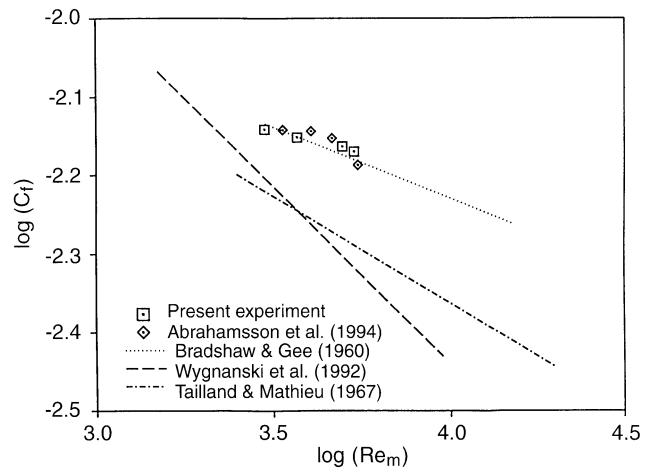


Fig. 11. Local skin friction coefficients. Comparison to literature data

investigations,  $C_f$  was determined from hot-wire measurements of the mean velocity near the surface, but using considerably larger values of  $y^+$  for the estimation. As was shown earlier, the velocity near the wall is not strictly linear beyond  $y^+ \approx 3$ .

### 3.2.5

#### Momentum balance

LR81 suggested that the two-dimensional momentum integral equation be used as the principal test for two-dimensionality. To second order, this equation reads

$$\int_0^{\infty} (U^2 + u^2 - v^2) dy = M_0 - \int_0^x (\tau_w / \rho) dx \quad (3.2)$$

where  $M_0$  is calculated according to

$$M_0 = \int_0^b U_{\text{inlet}}^2(y) dy \quad (3.3)$$

using the actual inlet velocity profile given in Fig. 3. Following Hussein et al. (1994), we can split the first integral in Eq. (3.2) in two parts according to

$$\int_0^{\infty} (U^2 + u^2 - v^2) dy = \int_0^{y(U=0)} + \int_{y(U=0)}^{\infty} = M_{\text{jet}} + M_{\text{return}} \quad (3.4)$$

For convenience, we may define

$$M_{\text{loss}} = \int_0^x (\tau_w / \rho) dx \quad (3.5)$$

The momentum integral equation can now be written as

$$(M_{\text{jet}} + M_{\text{return}}) / M_0 = 1 - M_{\text{loss}} / M_0 \quad (3.6)$$

A momentum balance is presented in Fig. 12. It is seen that the wall jet very well fulfils the momentum equation to  $x/b = 100$ . At  $x/b = 150$ , the jet momentum may have started to drop, and at  $x/b = 200$  we have a significant drop in jet momentum, meaning that the jet has started to lose momentum to the return flow. The somewhat larger discrepancy at  $x/b = 5, 10$  can probably be attributed to the fact that at these positions, the velocity profiles were not very well resolved and that measurements were stopped before the edge of jet was reached.

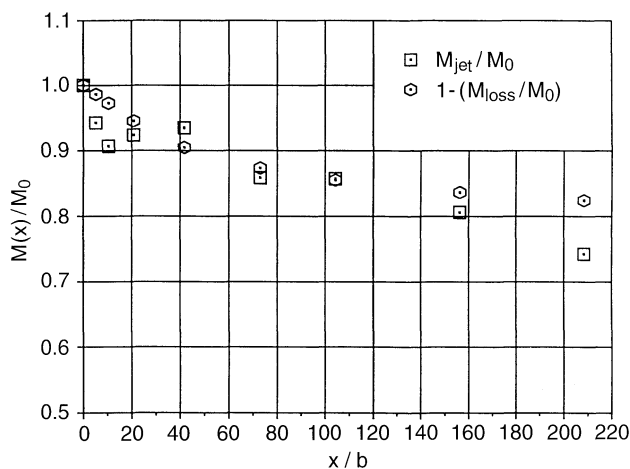


Fig. 12. Momentum balance

In conclusion, the momentum balance indicates that the flow is indeed a two-dimensional wall jet up to, and including, the streamwise position  $x/b = 150$ .

### 3.3

#### The developed region in inner variables

##### 3.3.1

##### Mean velocity

Figure 13 shows the mean velocity profiles from  $x/b = 40$  to  $x/b = 150$  in inner scaling ( $U^+ = U/u^*$ ,  $y^+ = yu^*/\nu$ ,  $u^* = \sqrt{\tau_w/\rho}$ ). These profiles appear to collapse well for  $y^+ \leq 100-200$ , which gives credibility to the wall shear stress measurements since any non-systematic errors in these measurements would tend to pull the profiles apart. The  $x/b = 200$ -profile, not shown here, deviates from the rest of the profiles for  $y^+ \geq 10$ .

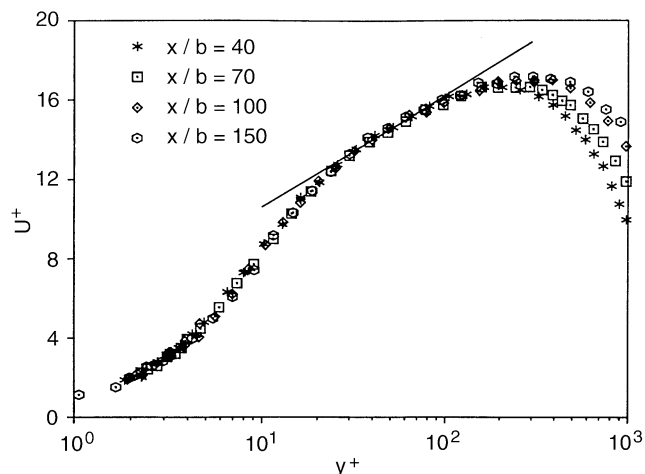
The straight line  $U^+ = 2.44 \times \ln y^+ + 5.0$  (i.e. the generally accepted relation for the flat plate boundary layer) is drawn in Fig. 13. This logarithmic line coincides with the experimental points for only a short interval in  $y^+$ . Plotting each profile separately, not shown here for the sake of brevity, one finds that the logarithmic line fits the data well over the interval  $30 \leq y^+ \leq 80$  for the first two streamwise positions. At  $x/b = 100$ , there is still an acceptable fit, albeit over a smaller portion of the profile. For the  $x/b = 150$  - profile, the situation is more unclear. A line with a different slope might give a good fit to the data over a part of the profile slightly further out from the wall.

These profiles have been analyzed extensively by GAELK who argue for a power law  $U^+ \sim C_i(y^+ + a^+)^{\gamma}$ , where  $a^+ \approx -30$  and  $\gamma$  and  $C_i$  depend on  $y_{1/2}^+$ . They conclude that a power law relation is more consistent with the data than the normal log law.

##### 3.3.2

##### Turbulence quantities

The turbulence intensity and shear stress measurements are shown in Figs. 14a-c. Contrary to Figs. 8a-c, no attempt has been made to correct for the influence of the return flow. (Since

Fig. 13. Mean velocity profiles in inner scaling,  $U^+ = f(y^+)$ . Line showing logarithmic velocity distribution included

we see no way of, with any degree of certainty, quantitatively estimating the influence on the inner part of the jet.)

The scaled streamwise turbulence intensity  $(u')^+$  is clearly dependent on streamwise position (or Reynolds number) outside  $y^+ \approx 8$ , the inner peak level increasing from  $\approx 2.9$  to  $\approx 3.4$ . It cannot be ruled out that this is partly due to the influence of the return flow, but it is highly improbable that it should be due entirely to this. The two upstream profiles have essentially the same turbulence level in the outer layer. The two downstream profiles may be influenced, but correcting in the same way as for the outer layer would still leave a difference in  $(u')^+$ . This dependence might rather be interpreted as a Reynolds number effect. It has been shown (Gad-el-Hak and Bandyopadhyay 1994, So et al. 1996) that  $Re$ -number effects penetrate much deeper in terms of turbulence intensities than for the mean velocity, and the  $Re$ -number of the inner layer of the wall jet does increase with increasing  $x$ .

The inner peak levels reported here are higher than the peak levels reported for other wall-bounded flows. A few examples of reported peak  $(u')^+$ -levels are 2.7 for a flat plate boundary layer (Karlsson and Johansson 1988), 2.55 for channel flow (Durst et al. 1996) and 2.7 for pipe flow (Durst et al. 1996), as compared to approximately 3.1 for the  $x/b = 70$ -position of the wall jet. An energy budget is required to completely explain the higher levels in the wall jet, but part of the explanation is probably the fact that there are in the wall jet two peaks in the  $\overline{u^2}$ -profile with rather high levels in between, meaning that the outward transport from the inner peak will be smaller. The peak level positions are found in the range  $y^+ = 15-20$ . There might be a weak tendency of outward movement of the peak position with increasing streamwise distance.

The scaled normal turbulence intensity  $(v')^+$  collapses out to  $y^+ \approx 30$ . In contrast to  $(u')^+$ , there is no inner peak, but something that looks like an inflexion point can be seen around  $y^+ = 50-60$ . It is also seen that  $(v')^+$  tends to a finite value ( $\approx 0.1$ ) as  $y^+ \rightarrow 0$ , indicating the presence of noise in the data.

We may use the observed collapse in  $(v')^+$  to estimate the maximum penetration of the disturbance from the return flow. Experience from other wall-bounded flows (Gad-el-Hak and

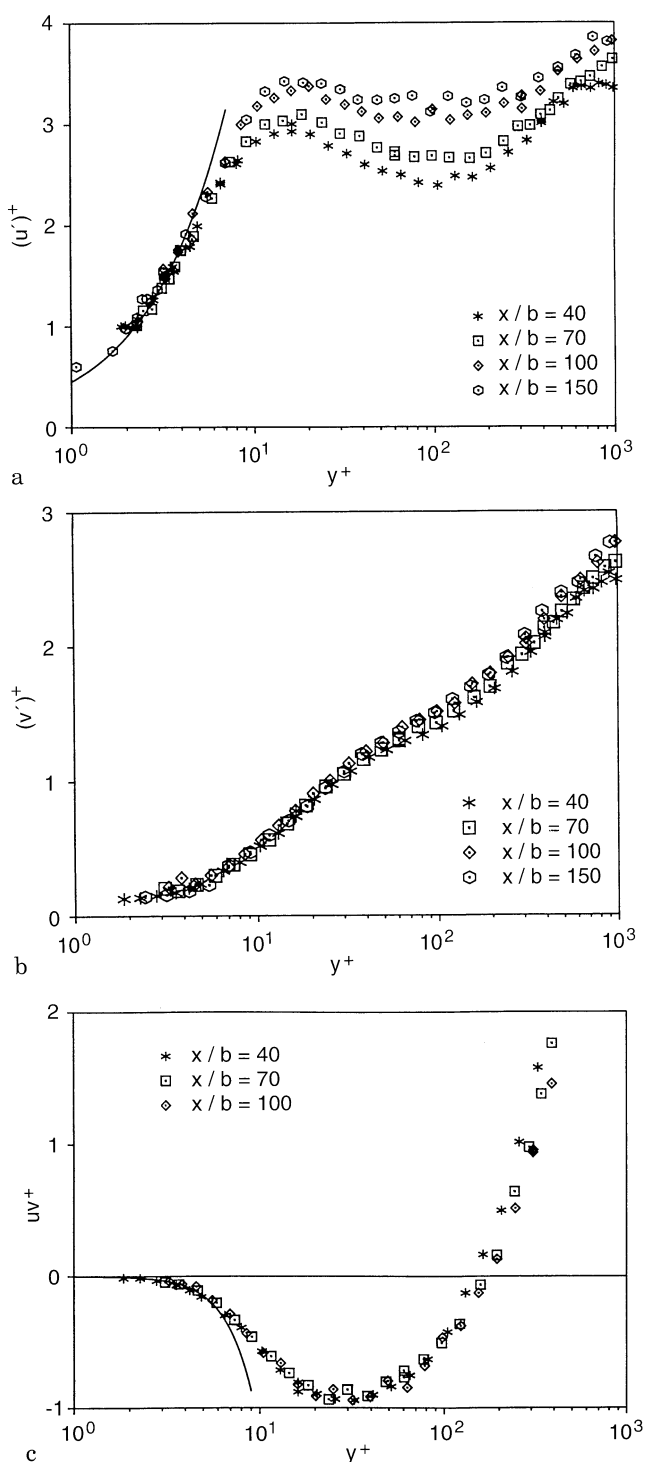


Fig. 14. Turbulence quantities in inner scaling. a  $\sqrt{u'^2}/u^*$ ; b  $\sqrt{v'^2}/u^*$ ; c  $\overline{uv}/u^{*2}$

Bandyopadhyay, 1994) indicates that if there is a change in  $(v')^+$  (or  $(u')^+$ ) vs.  $y^+$  with  $Re$ -nr, then  $(v')^+$  increases with increasing  $Re$ -nr. The influence of the return flow is similar in the sense that it too causes an increase in  $(v')^+$  (and  $(u')^+$ ) with increasing streamwise position. But since we observe no increase in  $(v')^+$  below  $y^+ \approx 30$ , none of the effects will exist below that position. (At least no effects that can be seen in this

resolution of Fig. 14b.) Alternatively, it may be argued that below this position, any effects of the outer flow are only reflected in  $u^*$  itself. Whichever, we can estimate the lower limit of influence of the return flow to  $y^+ \approx 30$ , lower limit meaning that the influence might start further out but it cannot be seen further in.

With the exception of the  $x/b = 150$  – profile, the non-dimensionalized shear stress  $(\overline{uv})^+$  collapses out to  $y^+ \approx 100$ . The inner peak level is close to  $-1$  ( $\approx -0.93$ ), in sharp contrast to the value of  $\approx -0.25$  reported by Abrahamsson et al. A short region with approximately constant Reynolds stress, ranging from  $y^+ \approx 20$  to  $y^+ \approx 40$ , is clearly seen. Furthermore, a close comparison of Figs. 13 and 14c reveals the often-mentioned fact that the position where  $\overline{uv} = 0$  does not coincide with the position where  $U = U_m$ , the former being closer to the wall than the latter.

Also shown in Fig. 14 are our best estimates of the leading terms in the near-wall series expansions of  $(u')^+$  and  $(\overline{uv})^+$ , i.e.  $a_u y^+$  and  $a_{uv} y^+$ . We estimate  $a_u = 0.45 \pm 0.02$ , which is significantly higher than corresponding experimental values for the flat plate boundary layer,  $0.39 \pm 0.01$  according to Johansson and Karlsson (1989), or channel flow,  $0.40$  according to Alfredsson et al. (1988). On the other hand, So et al. (1996), using turbulence modelling, have shown that in the limit of high  $Re$ -numbers,  $a_u$  is close to  $0.45$  for the flat plate boundary layer as well.  $a_{uv}$  is estimated to  $-0.0012$ . The actual measurements points to a value somewhere between  $-0.0011$  and  $-0.0015$ .  $-0.0012$  is chosen as a value consistent with the estimate of the fourth order term in the expansion of the mean velocity. ( $a_{uv} = 4c_4$  from the momentum equation near the wall.) The near-wall data for  $(v')^+$ , which admittedly are uncertain, points to  $a_v \approx 0.02$ . This value is about twice as large as earlier reported for other flows, e.g. Karlsson (1993) for a flat plate boundary layer or the review article by So et al. (1991).

#### 4 Summary and conclusions

An experimental study of the flow field in a two-dimensional, plane turbulent wall jet at an inlet Reynolds number of 9600 has been carried out using two-component LDV. The experiment has been shown to be momentum conserving to the streamwise position  $x/b = 150$ . Particular attention was given to the inner region of the flow, where the small measuring control volume and the optical arrangement of the LDV system permitted measurements of  $U$  and  $u'$  down to  $y^+ = 1-2$  and measurements of  $v'$  and  $\overline{uv}$  down to  $y^+ = 2-3$ , depending on streamwise position.

Wall shear stresses were determined directly from the mean velocity gradient in the viscous sublayer using only data below  $y^+ = 3-4$ . Above  $y^+ \approx 3$ , the velocity profile is no longer strictly linear. The results were in reasonable agreement with Preston tube measurements, but not with HWA measurements which were significantly lower. The failure of the HW was attributed to the fact that estimates were based on measurements considerably further from the wall. Perhaps some of the shear stresses from earlier data can be recomputed using the higher term for the Taylor expansion of the velocity near the wall presented here.

The data in the range  $40 \leq x/b \leq 150$  was found to be reasonably consistent with similarity. The mean velocity profiles are self-similar in inner scaling out to  $y^+ \leq 100$ –200, whereas the turbulence quantities shows similarity over a considerably shorter range in  $y^+$ . The  $(u')^+$ -profiles collapses out to  $y^+ \approx 8$ , the  $(v')^+$ -profiles out to  $y^+ \approx 30$  and the  $(\overline{uv})^+$ -profiles out to  $y^+ \approx 100$ . The GAELK similarity constraint  $U_m \sim (y_{1/2})^n$  was fulfilled for  $40 \leq x/b \leq 150$ .

Earlier stationary HWA measurements of  $v'$  and  $\overline{uv}$  were shown to be in error for  $y > \sim 0.5 \times y_{1/2}$ . The differences could be attributed to problems of stationary hot-wires in high intensity flows.

The near wall region of the turbulent wall jet has been resolved for the first time, including the inner, negative, peak in the shear stress. The inner peak levels of the streamwise turbulence intensity,  $(u')^+$ , were found to be higher than the peak levels reported for other wall-bounded flows. The limiting values of  $(u')^+$  and  $uv^+$  were determined, the latter being in good agreement with the second term in the near-wall series expansion of  $U^+$ .

### Appendix: Data corrections

The data presented here have been corrected for various error sources. These error sources are non-orthogonalities, gradient broadening and system noise. The two latter are of importance in the near-wall region only. Non-orthogonality effects are not restricted to that region. An exhaustive discussion of the applied corrections is given in Eriksson et al. (1997). In short, non-orthogonalities are treated using the methodology of Karlsson et al. (1993a), whereas the methodology for gradient broadening – correction essentially is an adoption from Durst et al. (1993).

### References

- Abrahamsson H** (1997) On turbulent wall jets. Ph.D. Thesis, Chalmers University of Technology, Gothenburg, Sweden
- Abrahamsson H; Johansson B; Löfdahl L** (1994) A turbulent plane two-dimensional wall jet in a quiescent surrounding. *European Journal of Mechanics B. Fluids* 13: 533–556
- Alfredsson PH; Johansson AV; Haritonidis JH; Eckelmann H** (1988) The fluctuating wall-shear stress and velocity field in the viscous sublayer. *Physics of Fluids* 31: 1026–1033
- Bradshaw P; Gee MT** (1960) Turbulent wall jets with and without an external stream. *Aeronautical Research Council R&M* 3252
- Buchhave P** (1975) Biasing errors in individual particle measurements with the LDA-counter signal processor. *Proceedings of the LDA-Symposium Copenhagen 1975*, Dantec Measurement Technology, Skovlunde, Denmark
- Buchhave P** (1979) The measurement of turbulence with the burst-type laser doppler anemometer – errors and correction Methods. Ph.D. Thesis, State University of New York at Buffalo
- Durst F; Kikura H; Lekakis I; Jovanovic J; Ye O** (1996) Wall shear stress determination from near-wall mean velocity data in turbulent pipe and channel flow. *Exp Fluids* 20: 417–428
- Durst F; Jovanovic J; Sender J** (1993) Detailed measurements of the near-wall region of turbulent pipe flow. *ASME Fluids Engineering Symposium*, Washington DC, USA
- Eriksson J; Karlsson R; Persson J** (1997) An experimental study of a two-dimensional plane turbulent wall jet. Report US 97:17Ö Vattenfall Utveckling AB, Älvkarleby, Sweden
- Gad-el-Hak M; Bandyopadhyay PR** (1994) Reynolds number effects in wall-bounded turbulent flows. *Appl Mech Rev* 47: 307–365
- George WK; Abrahamsson H; Eriksson J; Löfdahl L; Karlsson R** (1997) A similarity theory for the plane turbulent wall jet, Submitted for publication. Also: Internal Report 97/7, Dept. of Thermo and Fluid Dynamics, Chalmers University of Technology, Gothenburg Sweden
- George WK; Abrahamsson H; Löfdahl L** (1996) A similarity theory for the plane wall jet, Paper presented at the 3rd International Symposium on Engineering Turbulence Modelling and Measurements, Heraklion-Crete, Greece
- Hussein HJ; Capp SP; George WK** (1994) Velocity measurements in a High-Reynolds-Number Momentum-Conserving, Axisymmetric, Turbulent Jet. *J Fluid Mech* 258: 31–75
- Johansson TG; Karlsson RI** (1989) The energy budget in the near-wall region of a turbulent boundary layer. *Applications of Laser Anemometry to Fluid Mechanics*, (Adrian RJ et al. editor) Springer, Berlin, Heidelberg, pp 3–22
- Johnson DA; Brown D** (1990) A laser doppler velocimeter approach for near-wall three-dimensional turbulence measurements, Paper 3.2. In: *Fifth Int Symp on Applications of Laser Techniques to Fluid Mechanics*, Lisbon, Portugal
- Karlsson RI** (1993) Near-wall measurements of turbulence structure in boundary layers and wall jets near-wall turbulent flows, eds. RMC So et al., Elsevier, Amsterdam, pp 423–432
- Karlsson RI; Johansson TG** (1988) LDV measurements of higher order moments of velocity fluctuations in a turbulent boundary layer. *Laser Anemometry in Fluid Mechanics III*, Eds. RJ Adrian et al. Ladoan – Instituto Superior Tecnico, Lisbon
- Karlsson RI; Eriksson J; Persson J** (1993a) LDV measurements in a plane wall jet in a large enclosure. *Laser techniques and applications in fluid mechanics*, Eds. RJ Adrian et al., Springer, Berlin-Heidelberg, pp 311–332
- Karlsson RI; Eriksson J; Persson J** (1993b) An experimental study of a two-dimensional plane turbulent wall jet. Report VU-S 93:B36, Vattenfall Utveckling AB
- Lauder BE; Rodi W** (1981) The turbulent wall jet. *Prog Aerospace Sci* 19: 81–128
- Lauder BE; Rodi W** (1983) The turbulent wall jet – measurements and modelling. *Ann Rev Fluid Mech* 15: 429–459
- Meyers JF; Clemmons JI** (1979) Processing laser velocimeter high-speed counter data. *Laser velocimetry and particle sizing* (Thompson HD; Stevenson WH editor) Hemisphere Publishing Co., Washington, pp 300–313
- Morel T** (1975) Comprehensive design of axisymmetric wind tunnel contractions. *J Fluids Eng* 97: 225–233
- Schneider ME** (1987) Laser-Doppler measurements of turbulence in a two-dimensional wall jet on a flat plate in stagnant surroundings. Ph.D. Thesis, University of Minnesota
- Schneider ME; Goldstein RJ** (1994) Laser Doppler measurement of turbulence parameters in a two-dimensional plane wall jet. *Phys Fluids* 6: 3116–3129
- So RMC; Aksoy H; Yun SP; Sommer TP** (1996) Modelling Reynolds-number effects in wall-bounded turbulent flows. *J Fluids Eng* 118: 260–267
- So RMC; Lai YG; Zhang HS; Hwang BG** (1991) Second-order near-wall turbulence closures: A review. *AIAA J* 29: 1819–1835
- Tailland A; Mathieu J** (1967) Jet pariétal. *Journal de Mécanique* 6: 103–131
- Whiffen MC** (1975) Polar response of an LV measurement volume, *Minnesota Symposium on Laser Anemometry*, University of Minnesota, Minneapolis
- Wyganski J; Katz Y; Horev E** (1992) On the applicability of various scaling laws to the turbulent wall jet. *J Fluid Mech* 234: 669–690